2008 IEEE International Conference on
Robotics and Automation
Pasadena, CA, USA, May 19-23, 2008

C-Space Characterization of Contact Preserving Paths with Application to Tactile-Sensor Based Mobile Robot Navigation

Yoav Gabriely and Elon Rimon

Abstract— **This paper considers the navigation of a three degrees-of-freedom mobile robot equipped with position and tactile sensors in an unknown planar environment. The paper focuses on the contact preserving segments of the robot's path. Any contact preserving path can trace a single or two simultaneous contacts. The paper establishes that motions involving two contacts induce two types of configuration-space curves: contractible loops representing passable gaps, and non-contractible loops representing impassable gaps. The paper identifies a generic class of contact preserving paths which requires only single-contact tracings with efficient transitions at double-contact configurations involving impassable gaps, and at triple-contact configurations involving both passable and impassable gaps. A preliminary tactile-sensor navigation algorithm based on these paths is illustrated with an example.**

I. INTRODUCTION

This paper considers the navigation of a three degrees-of-freedom mobile robot in a planar environment populated by unknown obstacles. The robot has no apriori information about the environment, but may locally acquire this information using its on-board sensors. This class of on-line problems has a wide range of applications in unstructured environments where the robot must detect obstacles during task execution. Examples are material and mail delivery in factories and offices [1], medicine distribution in hospitals [6], horticulture duty in greenhouses [8], and planetary exploration and sample acquisition [10], [14]. Current sensor-based navigation algorithms usually assume that the robot moves with two translational degrees of freedom (two exceptions are discussed below). However, practical mobile robots move with *three* degrees of freedom involving translation and rotation. Since full maneuverability is often critical for task completion, there is a need to develop sensor based navigation algorithms that can plan the robot's full three degrees of freedom motions.

Much like the classical sensor based navigation algorithms, this paper focuses on tactile-sensor based navigation. Two notable algorithms in this area are $BUG1$/$BUG2$ [15] and $ALG1$/$ALG2$ [17]. Both algorithms navigate a two degrees-of-freedom mobile robot in an unknown planar environment using position and tactile sensors. These works have been extended to navigation in planar environments using vision and laser sensors [11], [14], [18]. However, these works assume that the robot moves with two translational degrees of freedom. This paper strives to achieve tactile based navigation of three degrees-of-freedom mobile robots.

Yoav Gabriely and Elon Rimon are with the Department of Mechanical Engineering, Technion, Israel rimon@tx.technion.ac.il

Cox and Yap consider three degrees-of-freedom navigation of a rod equipped with position and tactile sensors in an unknown planar environment [5]. Once the rod hits a collection of impassable obstacles, it traces a series of double-contact curves until it can resume its motion toward the target. Their algorithm requires that the rod follow paths which maintain *two sliding contacts,* a demanding task that can only be implemented with very slow and guarded robot motions. Under our approach the mobile robot is a general convex body, and its contact preserving paths involve only *single-contact* tracings.

Choset et al. consider three degrees-of-freedom navigation of a convex robot equipped with position and distance-to-obstacles sensors in an unknown planar environment [3], [4]. The robot follows a c-space network of generalized Voronoi curves corresponding to equidistant configurations from triplets of obstacles in the environment. While this approach can be readily implemented, it requires that the robot be able to continuously observe triplets of obstacles in order to proceed along the generalized Voronoi curves. Moreover, these curves do not necessarily form a connected network, forcing the robot to follow possibly complex connection curves between the network's distinct components. Under our approach the robot moves along single obstacles in the environment, and only the transitions between successive path segments involve multiple contacts with the environment. Navigation along a single obstacle at a time seems to offer significant advantages in terms of path robustness and ease of implementation.

This paper reports initial results concerning tactile-sensor based navigation of a three degrees-of-freedom convex robot moving in a planar environment populated by unknown polygonal obstacles. The paper focuses on the robot's contact preserving path segments, where it attempts to efficiently circumnavigate collections of impassable obstacles.

The paper's structure and contributions are as follows. Section II generalizes a classical result on the existence of contact preserving paths between two contact configurations with a collection of impassable obstacles. Section III classifies the robot's double-contact paths in terms of two types of configuration-space curves: contractible loops representing passable gaps, and non-contractible loops representing impassable gaps. Based on this classification, Section IV identifies a minimal set of obstacles which supports contact preserving paths between any two contact configurations with a collection of impassable obstacles. This section also describes a generic class of contact preserving paths consisting only of single-contact tracing segments. Section V

describes a preliminary tactile-sensor based navigation algorithm together with an execution example. The concluding section discusses the generalization of the approach to remote-sensing obstacle detection sensors.

II. EXISTENCE OF CONTACT PRESERVING PATHS

This section describes our setup, then establishes a basic result on the existence of contact preserving paths. The robot is a *strictly convex* body denoted $\mathcal{A}$ having a piecewise smooth boundary. The robot moves with three degrees of freedom in a planar environment populated by stationary polygonal obstacles denoted $\mathcal{B}_0, \ldots, \mathcal{B}_m$. The perimeter of each obstacle is a simple *polygonal loop* such that one obstacle, say $\mathcal{B}_0$, surrounds the environment from the outside. The robot, having no apriori knowledge of the environment, is required to navigate to various targets using two sensors which are assumed ideal. The first is a position-and-orientation sensor giving the robot's coordinates with respect to a fixed reference frame. The second is a tactile sensor mounted along the robot's perimeter, giving the robot's current contact with the environment while monitoring establishment of new contacts. Based on these readings, the robot is capable of executing contact preserving paths as well as changing the contact being traced at discrete multi-contact configurations.

Next we introduce configuration space terminology. The mobile robot's *c-space* is the three-dimensional space $\mathbb{R}^2 \times S^1$, where S^1 is the unit circle. Points in $\mathbb{R}^2 \times S^1$ are denoted $q = (d, \theta)$, where $d = (d_x, d_y) \in \mathbb{R}^2$ and $\theta \in S^1$ are the robot's translational and rotational degrees of freedom. Let $\mathcal{A}(q)$ denote the set occupied by the robot when it is at a configuration q. The *c-obstacle* corresponding to $\mathcal{B}_i$, denoted $\mathcal{CB}_i$, is the set of configurations at which $\mathcal{A}(q)$ intersects $\mathcal{B}_i$. The boundary of $\mathcal{CB}_i$, denoted $\mathsf{bdy}(\mathcal{CB}_i)$, consists of configurations at which $\mathcal{A}(q)$ touches $\mathcal{B}_i$ such that the bodies' interiors are disjoint. It can be verified that $\mathcal{CB}_i$ is bounded by piecewise smooth surfaces. The free configuration space, denoted $\mathcal{F}$, is the complement of the c-obstacles' interiors.

We now consider a key theorem on the existence of contact preserving paths. Let the robot's *minimal width,* denoted D_{min}, be the minimal distance among all antipodal points along the robot's perimeter. A collection of impassable obstacles is a set of obstacles lying less than D_{min} apart, thus forming a single obstacle from the robot's perspective (see Section IV).

Theorem 1: Let a planar robot (not necessarily convex) move in a bounded planar environment. Let the robot touch a collection of impassable obstacles at two configurations q_1 and q_2. If there exists a path between q_1 and q_2 in $\mathcal{F}$, there exists a **contact preserving** path between q_1 and q_2 in $\mathcal{F}$.

Note that the contact preserving path can maintain contact with the collection of impassable obstacles as well as other neighboring obstacles. A version of the theorem for a convex body moving amidst convex parts appeared in the context of assembly planning [9]. We provide a general version of the theorem together with a new proof of the result.

Proof: By assumption q_1 and q_2 lie in the same connected component of $\mathcal{F}$. Hence we simply regard $\mathcal{F}$ as consisting of a single connected set. Since the physical environment is compact the free c-space $\mathcal{F}$ is compact in $\mathbb{R}^2 \times S^1$. The boundary of each c-obstacle consists of connected piecewise-smooth surfaces. Hence $\mathcal{F}$ itself is bounded by compact and connected piecewise-smooth surfaces, denoted $\mathcal{S}_0 \ldots \mathcal{S}_p$. For generic obstacle arrangements, each $\mathcal{S}_i$ is a compact and connected two-dimensional topological manifold in $\mathbb{R}^2 \times S^1$.

We now invoke the generalized Jordan curve theorem [2]. Every compact and connected two-dimensional topological manifold in $\mathbb{R}^2 \times S^1$ forms a closed surface which separates the ambient c-space into two disjoint connected sets: a bounded *interior set* enclosed within the surface, and an unbounded *exterior set* lying outside the surface. This theorem is formally discussed in Ref. [7] while some intuition is provided below.

Recall that $\mathcal{S}_0 \ldots \mathcal{S}_p$ denote the distinct boundary surfaces of $\mathcal{F}$. Since $\mathcal{F}$ is connected, it lies either within the interior or within the exterior of each surface $\mathcal{S}_i$ for $i = 0 \ldots p$. The set obtained by removing from $\mathbb{R}^2 \times S^1$ the interior of all surfaces $\mathcal{S}_0 \ldots \mathcal{S}_p$ is unbounded. Since $\mathcal{F}$ is bounded, it must lie in the interior of at least one surface, say $\mathcal{S}_0$. All other surfaces are subsets of $\mathcal{F}$ and therefore lie within the interior of $\mathcal{S}_0$. The connectivity of $\mathcal{F}$ now implies that it must lie in the exterior of all internal surfaces $\mathcal{S}_1 \ldots \mathcal{S}_p$. The c-obstacles therefore lie in the exterior of $\mathcal{S}_0$ and in the interior of each $\mathcal{S}_i$ for $i = 1 \ldots p$.

We now invoke a second result. If an obstacle is connected in physical space, its c-obstacle is connected in $\mathbb{R}^2 \times S^1$ [13, Prop. 2.6]. A collection of impassable obstacles induces overlapping c-obstacles whose union is similarly a connected set in $\mathbb{R}^2 \times S^1$. The exterior of $\mathcal{S}_0$ and the interior of each $\mathcal{S}_i$ $(i = 1 \ldots p)$ are disjoint sets. Since the union of the c-obstacles associated with a collection of impassable obstacles is connected, it lies either in the exterior of $\mathcal{S}_0$ or in the interior of some $\mathcal{S}_i$ for $1 \leq i \leq p$. Since q_1 and q_2 involve contact with the *same* collection of impassable obstacles, they lie on the same boundary surface $\mathcal{S}_i$ for some $0 \leq i \leq p$. Since each $\mathcal{S}_i$ is connected and consists of contact configurations, there exists a contact preserving path from q_1 to q_2. □

The original Jordan curve theorem asserts that every loop on a topological sphere separates the sphere into two sets. The same result holds for the cylinder $\mathbb{R} \times S^1$, which is analogous to our three-dimensional space $\mathbb{R}^2 \times S^1$. In contrast, the c-space of a 2R manipulator, being the torus $S^1 \times S^1$, does not possess such a separation property. Indeed, a 2R manipulator can touch an obstacle at two configurations connected by a collision-free path, yet there need not exist a contact preserving path between the two configurations. The implication of the theorem for tactile-based navigation is as follows. Given a target configuration, the mobile robot can initially move toward the target until it hits a collection of impassable obstacles. Based on the theorem, a tactile-based path can take the robot to any desired target along the obstacles' boundary

from which the robot can resume its motion towards the target. The characterization of an efficient contact-preserving path from a hit configuration to a leave configuration is discussed in the next section.

III. THE DOUBLE-CONTACT PATHS

We eventually synthesize contact preserving paths consisting of single-contact tracings with discrete transitions at double and triple-contact configurations. The double-contact configurations form a collection of curves in the robot's c-space. This section establishes that these curves belong to two topologically distinct classes associated with impassable and passable gaps.

In order to properly classify the double-contact curves, we decompose each polygonal obstacle $\mathcal{B}_i$ into a union of overlapping *convex* polygons. Let $\mathcal{B}_i$ consist of the union $\mathcal{B}_i = \cup_{j=1}^{k_i} \tilde{\mathcal{B}}_{i_j}$, such that each $\tilde{\mathcal{B}}_{i_j}$ is convex ($i = 0 \ldots m$). We require that every pair of overlapping convex pieces intersect *transversally,* at interior points of non-collinear edges. Note that there exist efficient algorithms for decomposing a given polygon into convex pieces [12][pp 197-216]. For notational simplicity, let $\tilde{\mathcal{B}}_1, \ldots, \tilde{\mathcal{B}}_k$ (where $k = \sum_{i=0}^{m} k_i$) denote the collection of all convex obstacle pieces in the environment. We also assume that $\mathcal{A}$'s boundary has a well defined normal at each of its points (the ensuing results hold true even when $\mathcal{A}$'s boundary is piecewise smooth).

The following lemma asserts that the robot's contact-point position with an obstacle induces a partition (or *foliation* [16]) of the c-obstacle boundary into a family of curves.

Lemma 3.1 (Contact-Point Foliation): Let the robot $\mathcal{A}$ be strictly convex and let $\tilde{\mathcal{B}}_i$ be a convex obstacle-piece. Then the surface of $\mathcal{C}\tilde{\mathcal{B}}_i$ is partitioned into one-dimensional curves, each associated with a **fixed contact point** along $\tilde{\mathcal{B}}_i$'s boundary:

$$\mathsf{bdy}(\mathcal{C}\tilde{\mathcal{B}}_i) = \cup_{x \in \mathsf{bdy}(\tilde{\mathcal{B}}_i)} \alpha_x \quad \text{s.t. } \alpha_x = \{q : \mathcal{A}(q) \cap \tilde{\mathcal{B}}_i = \{x\}\}.$$

Moreover, each α_x is monotonic and periodic in the θ-coordinate, but is aperiodic in the (d_x, d_y) coordinates.

Let us make two clarifying remarks. It can be verified that when $\mathcal{A}$ and $\tilde{\mathcal{B}}_i$ are convex, $\mathcal{C}\tilde{\mathcal{B}}_i$ is topologically equivalent to a solid cylinder parallel to the θ axis. Since θ is periodic in 2π, $\mathcal{C}\tilde{\mathcal{B}}_i$ is topologically equivalent to a solid torus in $\mathbb{R}^2 \times S^1$ (Figure 1). The periodicity of α_x in θ implies that it cannot be contracted to a point along the c-obstacle's surface. The aperiodicity of α_x in (d_x, d_y) means that it does not wrap around the solid cylinder corresponding to $\mathcal{C}\tilde{\mathcal{B}}_i$.

Proof sketch: Every $q \in \mathsf{bdy}(\mathcal{C}\tilde{\mathcal{B}}_i)$ corresponds to a configuration where $\mathcal{A}(q)$ touches $\tilde{\mathcal{B}}_i$ such that the bodies' interiors are disjoint. Since $\mathcal{A}$ is strictly convex and $\tilde{\mathcal{B}}_i$ is convex, $\mathcal{A}(q)$ touches $\tilde{\mathcal{B}}_i$ only at a single point. Hence every $q \in \mathsf{bdy}(\mathcal{C}\tilde{\mathcal{B}}_i)$ corresponds to a unique contact point $x \in \mathsf{bdy}(\tilde{\mathcal{B}}_i)$. It follows that the sets $\alpha_x = \{q : \mathcal{A}(q) \cap \tilde{\mathcal{B}}_i = \{x\}\}$ such that $x \in \mathsf{bdy}(\tilde{\mathcal{B}}_i)$ partition the surface of $\mathcal{C}\tilde{\mathcal{B}}_i$ into *disjoint* sets. A proof that each α_x forms a one-dimensional curve appears in [7]. Monotonicity and periodicity of α_x with respect to the robot's θ coordinate follows from the fact that both bodies are convex—one can monotonically rotate the robot while retaining contact with any fixed point $x \in \mathsf{bdy}(\tilde{\mathcal{B}}_i)$. A proof that α_x cannot wrap around $\mathcal{C}\tilde{\mathcal{B}}_i$ also appears in [7].

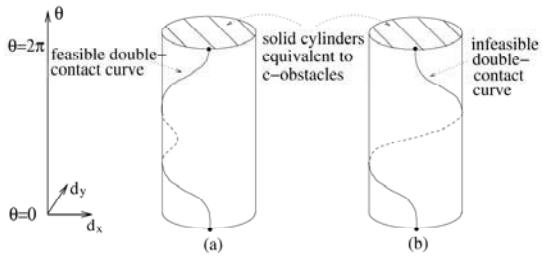

Fig. 1. (a) A topological model of a double-contact curve associated with an impassable gap. (b) An infeasible double-contact curve.

The following proposition asserts that impassable gaps induce non-contractible loops on the c-obstacles' surfaces. The minimal distance between $\tilde{\mathcal{B}}_i$ and $\tilde{\mathcal{B}}_j$ is denoted $\mathsf{dst}(\tilde{\mathcal{B}}_i, \tilde{\mathcal{B}}_j)$.

Proposition 3.2 (Impassable Gaps): Let the robot $\mathcal{A}$ be strictly convex, and let $\tilde{\mathcal{B}}_i$ and $\tilde{\mathcal{B}}_j$ be two possibly overlapping convex obstacle-pieces. Then $\tilde{\mathcal{B}}_i$ and $\tilde{\mathcal{B}}_j$ induce double-contact curves which are monotonic in θ and cross every fixed-θ slice of the robot's c-space iff

$$\mathsf{dst}(\tilde{\mathcal{B}}_i, \tilde{\mathcal{B}}_j) < D_{min},$$

where D_{min} is the robot's minimal width. Moreover, these double-contact curves are periodic in the θ coordinate but aperiodic in the (d_x, d_y) coordinates.

The curve's periodicity in θ implies that it forms a loop which cannot be contracted to a point along the surface of either c-obstacle. The curve's aperiodicity in (d_x, d_y) implies that it cannot wrap around either c-obstacle, see Figure 1. Due to space constraints, the proof of the proposition is relegated to Ref. [7]. The next proposition asserts that passable gaps induce contractible double-contact loops on the c-obstacles' surfaces. Let the robot's *maximal width,* denoted D_{max}, be the maximal distance over all antipodal points along the robot's perimeter.

Proposition 3.3 (Passable Gaps): Let the robot $\mathcal{A}$ be strictly convex, and let $\tilde{\mathcal{B}}_i$ and $\tilde{\mathcal{B}}_j$ be convex obstacle-pieces. Then $\tilde{\mathcal{B}}_i$ and $\tilde{\mathcal{B}}_j$ induce double-contact curves which cross only a subset of the fixed-θ slices of the robot's c-space iff

$$D_{min} < \mathsf{dst}(\tilde{\mathcal{B}}_i, \tilde{\mathcal{B}}_j) < D_{max},$$

where D_{min} and D_{max} are the robot's minimal and maximal widths. Moreover, these double-contact curves form loops which can be contracted to a point along the surface of either c-obstacle.

Due to space constraints, the proof of the proposition is also relegated to Ref. [7]. The following theorem summarizes the classification of the double-contact curves.

Theorem 2: Let the robot $\mathcal{A}$ be strictly convex, and let $\tilde{\mathcal{B}}_i$ and $\tilde{\mathcal{B}}_j$ be two convex obstacle-pieces. Then $\tilde{\mathcal{B}}_i$ and $\tilde{\mathcal{B}}_j$ induce two types of c-space double contact curves:

1. **Impassable gaps:** When $\mathsf{dst}(\tilde{\mathcal{B}}_i, \tilde{\mathcal{B}}_j) < D_{min}$ the double-contact curves form loops which cross every θ slice of $\mathbb{R}^2 \times S^1$, such that each loop is non-contractible on the

surface of either c-obstacle.

2. **Passable gaps:** When $D_{min} < \mathsf{dst}(\tilde{\mathcal{B}}_i, \tilde{\mathcal{B}}_j) < D_{max}$ the double-contact curves form loops which cross only a subset of the θ slices of $\mathbb{R}^2 \times S^1$, such that each loop is contractible to a point on the surface of either c-obstacle.

Note that triple-contact configurations, associated with simultaneous contact of the robot with three obstacle pieces, occur at points where *three* double-contact curves meet.

IV. A CLASS OF SIMPLE CONTACT PRESERVING PATHS

Recall that we wish to circumnavigate every collection of impassable obstacles using only single-contact tracings. This section characterizes a class of such paths which strives to minimize the number of contact-point transitions during the robot's motion. We first define what constitutes a collection of impassable obstacles. The convex obstacle pieces $\tilde{\mathcal{B}}_1, \ldots, \tilde{\mathcal{B}}_m$ are simply called 'obstacles' for the remainder of the paper.

Definition 1: A single obstacle $\tilde{\mathcal{B}}_i$ is impassable. A collection of p obstacles $\boldsymbol{\mathcal{B}} = \{\tilde{\mathcal{B}}_1, \ldots, \tilde{\mathcal{B}}_p\}$ such that $p > 1$ is **impassable** if $\cup_{j=1}^{p-1} \tilde{\mathcal{B}}_j$ is impassable and $\mathsf{dst}\big(\tilde{\mathcal{B}}_p, \cup_{j=1}^{p-1} \tilde{\mathcal{B}}_j\big) < D_{min}$, where D_{min} is the robot's minimal width.

Each collection of impassable obstacles forms a connected graph. Its nodes are the obstacles of $\boldsymbol{\mathcal{B}}$, and its edges connect obstacles which either overlap or share an impassable gap. The next definition augments a collection of impassable obstacles with triple-contact neighbors.

Definition 2: Let $\boldsymbol{\mathcal{B}}$ be a collection of impassable obstacles. The **3-connected set** of $\boldsymbol{\mathcal{B}}$, denoted $\bar{\boldsymbol{\mathcal{B}}}$, is constructed as follows.

1. Initialize $\bar{\boldsymbol{\mathcal{B}}}$ with the obstacles of $\boldsymbol{\mathcal{B}}$.

2. Repeat the following step:

2.1 Add a new obstacle $\tilde{\mathcal{B}}_i$ to $\bar{\boldsymbol{\mathcal{B}}}$ if there exist $\tilde{\mathcal{B}}_j, \tilde{\mathcal{B}}_k \in \bar{\boldsymbol{\mathcal{B}}}$ s.t. $\mathcal{A}$ can simultaneously touch $\tilde{\mathcal{B}}_i, \tilde{\mathcal{B}}_j, \tilde{\mathcal{B}}_k$. Then add to $\bar{\boldsymbol{\mathcal{B}}}$ all new obstacles $\tilde{\mathcal{B}}_l$ satisfying $\mathsf{dst}(\tilde{\mathcal{B}}_l, \tilde{\mathcal{B}}_i) < D_{min}$.

2.2 Add two new obstacles $\tilde{\mathcal{B}}_i, \tilde{\mathcal{B}}_j$ to $\bar{\boldsymbol{\mathcal{B}}}$ if there exists $\tilde{\mathcal{B}}_k \in \bar{\boldsymbol{\mathcal{B}}}$ s.t. $\mathcal{A}$ can simultaneously touch $\tilde{\mathcal{B}}_i, \tilde{\mathcal{B}}_j, \tilde{\mathcal{B}}_k$. Then add to $\bar{\boldsymbol{\mathcal{B}}}$ all new obstacles $\tilde{\mathcal{B}}_l$ satisfying either $\mathsf{dst}(\tilde{\mathcal{B}}_l, \tilde{\mathcal{B}}_i) < D_{min}$ or $\mathsf{dst}(\tilde{\mathcal{B}}_l, \tilde{\mathcal{B}}_j) < D_{min}$.

3. End when no new obstacles can be added to $\bar{\boldsymbol{\mathcal{B}}}$.

Each step of the construction adds to the current $\bar{\boldsymbol{\mathcal{B}}}$ new triple-contact neighbors, as well as new obstacles sharing an impassable gap with the new triple-contact neighbors. The set $\bar{\boldsymbol{\mathcal{B}}}$ can be represented by a connected graph, denoted $G\bar{\boldsymbol{\mathcal{B}}}$, as follows. Initially $G\bar{\boldsymbol{\mathcal{B}}}$ consists of the connected graph representing $\boldsymbol{\mathcal{B}}$. In step 2 we add a node for each new triple-contact neighbor, together with three edges $\tilde{\mathcal{B}}_i$–$\tilde{\mathcal{B}}_j$, $\tilde{\mathcal{B}}_i$–$\tilde{\mathcal{B}}_k$, $\tilde{\mathcal{B}}_j$–$\tilde{\mathcal{B}}_k$ between the obstacles involved in the triple contact. Then we add a node for each $\tilde{\mathcal{B}}_l$ with an edge to the obstacle with which it shares an impassable gap. The following key theorem asserts that the obstacles of $\bar{\boldsymbol{\mathcal{B}}}$ support contact preserving paths between the obstacles of $\boldsymbol{\mathcal{B}}$.

Theorem 3: Let q_1 and q_2 be two contact configurations of $\mathcal{A}$ with a collection of impassable obstacles $\boldsymbol{\mathcal{B}}$. If there exists a path from q_1 to q_2 in $\mathcal{F}$, there exists a contact preserving path from q_1 to q_2 which maintains contact only with the obstacles of the 3-connected set $\bar{\boldsymbol{\mathcal{B}}}$.

Moreover, $\bar{\boldsymbol{\mathcal{B}}}$ is minimal in the sense that in some environments a contact preserving path from q_1 to q_2 need not exist once an obstacle is removed from $\bar{\boldsymbol{\mathcal{B}}}$.

Due to space constraints, the proof of the theorem is relegated to Ref. [7]. The implication of the theorem for path synthesis is stated in the following corollary.

Corollary 4.1: Let q_1 and q_2 be two contact configurations of $\mathcal{A}$ with a collection of impassable obstacles $\boldsymbol{\mathcal{B}}$. There exists a path from q_1 to q_2 consisting only of single-contact tracings along $\bar{\boldsymbol{\mathcal{B}}}$'s obstacles, with transitions at configurations where $\mathcal{A}$ touches two obstacles of $\bar{\boldsymbol{\mathcal{B}}}$ sharing an impassable gap, or at configurations where $\mathcal{A}$ touches three obstacles of $\bar{\boldsymbol{\mathcal{B}}}$ sharing passable or impassable gaps.

V. A TACTILE SENSOR BASED NAVIGATION ALGORITHM

We describe a preliminary navigation algorithm for a three-degrees-of-freedom convex mobile robot which moves in a planar environment populated by unknown polygonal obstacles. The robot is equipped with tactile and position sensors, and has on-board memory which allows storage of the c-space curves constructed on-line by the algorithm.

We first sketch the global operation of the algorithm. Let S and T denote the robot's start and target configurations. Let P denote the fixed c-space plane parallel to the θ axis and containing S and T. The robot initially moves within P along a straight line from S to T, until it encounters a collection of impassable obstacles at a configuration q_1. Let $\boldsymbol{\mathcal{B}}$ be this collection of impassable obstacles, let $\bar{\boldsymbol{\mathcal{B}}}$ be its 3-connected set, and recall that $\mathcal{C}\bar{\boldsymbol{\mathcal{B}}}$ is the union of $\bar{\boldsymbol{\mathcal{B}}}$'s c-obstacles. The robot next executes a series of single-contact tracings along the obstacles of $\bar{\boldsymbol{\mathcal{B}}}$ while searching a network of c-space curves on $\mathcal{C}\bar{\boldsymbol{\mathcal{B}}}$'s surface. Using any standard search method such as DFS, the robot eventually reaches a configuration q_2 which lies in P and is closer to T then q_1. At this point the robot resumes its motion toward the target within P, until it encounters the next collection of impassable obstacles or reaches the target.

The robot's tactile sensor allows exploration of $\mathcal{C}\bar{\boldsymbol{\mathcal{B}}}$'s surface as follows. Recall that the contact-point position along a physical obstacle boundary partitions the c-obstacle's surface into one-dimensional curves or *leafs* (Lemma 3.1). On the other hand, the double-contact curves partition $\mathcal{C}\bar{\boldsymbol{\mathcal{B}}}$'s surface into two-dimensional sets or *cells* (each cell lies on the surface of an individual c-obstacle). Each cell is therefore a union of disjoint leaf segments, such that each leaf segment has its endpoints on double-contact curves. The latter endpoints occur at configurations at which the robot touches the current obstacle as well as some other neighboring obstacle. The robot can therefore trace an entire leaf segment by rotating its body in both directions while

maintaining the contact point fixed, until its tactile sensor reports that a new contact has been established. By repeating this process for each contact point along the physical obstacle boundary, the robot can explore an entire cell. In practice each leaf segment can be explored without any physical motion of the robot: one simply replaces the tactile sensor with an obstacle detection sensor capable of reporting on obstacles lying within the disc enclosing the robot at its current position.

We now focus on the incremental construction of the network of c-space curves on $\mathcal{C}\bar{\mathcal{B}}$'s surface, denoted $\mathcal{R}(\bar{\mathcal{B}})$. Each curve of $\mathcal{R}(\bar{\mathcal{B}})$ corresponds to a single-contact tracing along an obstacle of $\bar{\mathcal{B}}$. During this tracing the robot monotonically advances its contact point, denoted x, along the obstacle's boundary. Each position of x is associated with a particular leaf segment as described above. Using its tactile sensor, the robot determines for each x the interval $[\theta_{min}(x), \theta_{max}(x)]$ which bounds the leaf-segment's θ coordinate. If at a particular x the robot can perform full rotation without touching other obstacles, $[\theta_{min}(x), \theta_{max}(x)] = [0, 2\pi]$. As the robot traces an obstacle boundary, it moves with orientation $\theta(x) \in [\theta_{min}(x), \theta_{max}(x)]$ which minimizes its clearance with respect to the obstacle's boundary (Figure 2). The c-space curve associated with each single-contact tracing forms a *skeletal curve* of the current cell.

The vertices of $\mathcal{R}(\bar{\mathcal{B}})$ are of the following three types. The first two types occur when the interval $[\theta_{min}(x), \theta_{max}(x)]$ shrinks along a skeletal curve to a single point. This event occurs when the monotonic tracing of x along the current obstacle boundary wedges the robot against two or three obstacles. The first type of vertex occurs when the robot finds itself wedged against three obstacles. This configuration becomes a *triple-contact vertex* of $\mathcal{R}(\bar{\mathcal{B}})$. Three double-contact curves meet at this vertex, and these curves bound three cells which share the vertex as their common boundary. Each of the three cells has a skeletal curve emanating from the vertex. When the robot reaches the vertex, it "jumps" the contact x to one of the two neighboring obstacles, then proceeds to trace the neighboring obstacle boundary.

The second type of vertex occurs when the robot reaches a point where it finds itself wedged against two obstacles. It can be verified that this event is associated with an impassable gap. The robot has thus reached a double-contact curve associated with an impassable gap. The wedging configuration, denoted q', becomes a *double-contact vertex* of $\mathcal{R}(\bar{\mathcal{B}})$. While the leaf segment of the current cell has shrunk to a single point at q', a leaf segment on the neighboring c-obstacle surface also passes through q'. Only one additional curve of $\mathcal{R}(\bar{\mathcal{B}})$ emanates from q' as follows. This curve initially follows the leaf segment on the neighboring c-obstacle surface from q' to its minimum-clearance configuration on the leaf segment, then continues along the skeletal curve lying on the neighboring c-obstacle surface. Physically the robot "jumps" the contact to a new point x lying on the neighboring obstacle sharing the impassable gap, rotates against the new obstacle until reaching its minimum-clearance orientation, then proceeds to trace the neighboring obstacle boundary.

The third type of vertex occurs when the robot reaches a point x'' at which the interval $[\theta_{min}(x''), \theta_{max}(x'')]$ splits into two intervals which become separated as the robot continues its tracing of the current obstacle boundary. In c-space this event occurs when the current skeletal curve reaches a leaf segment which is tangent to a double-contact curve at a configuration denoted q''. As the robot continues the tracing of x along the current obstacle boundary, the tangent leaf-segment splits into two separate leaf-segments on the current c-obstacle surface. The endpoint of the current skeletal curve becomes a *split vertex* of $\mathcal{R}(\bar{\mathcal{B}})$, and two new curves of $\mathcal{R}(\bar{\mathcal{B}})$ emanate from this vertex. These curves initially follow the tangent leaf-segment in either direction, then proceed along the skeletal curves of the two cells lying on the current c-obstacle surface beyond the tangent leaf-segment. Physically, when the robot reaches x'' it detects for the first time a neighboring obstacle. While the robot can continue its monotonic tracing of x along the current obstacle boundary, the neighboring obstacle forces the robot to choose between two possible θ-intervals in order to proceed with the tracing beyond x''. Note that the robot continues the tracing of x along the *current* obstacle boundary as it passes through a split vertex.

To summarize, a network $\mathcal{R}(\bar{\mathcal{B}})$ is constructed incrementally on $\mathcal{C}\bar{\mathcal{B}}$'s surface starting from a hit configuration q_1. The network's curves correspond to single-contact tracings. Its vertices are triple-contact configurations, double-contact configurations associated with impassable gaps, and split vertices associated with the appearance of neighboring obstacles. A future paper will formally establish that $\mathcal{R}(\bar{\mathcal{B}})$ visits every cell on $\mathcal{C}\bar{\mathcal{B}}$'s surface, and also crosses the plane P at a configuration q_2 which is closer to T than q_1.

Execution example: Figure 2 shows an ellipse robot which has to navigate to a target T in an unknown environment consisting of a composite obstacle $\mathcal{B}_1$ and two convex obstacles $\mathcal{B}_2$ and $\mathcal{B}_3$. Note that the 3-connected set of $\mathcal{B}_1$ includes both obstacles $\mathcal{B}_2$ and $\mathcal{B}_3$. The robot initially moves toward T until it hits $\mathcal{B}_1$ at a configuration q_1 (Figure 2(a)). It rotates to a minimum-clearance orientation, then proceeds to trace the boundary of $\mathcal{B}_1$. This motion eventually wedges the robot against two obstacle-pieces of $\mathcal{B}_1$ (Figure 2(a)). This is a double-contact vertex of $\mathcal{R}(\bar{\mathcal{B}})$, and the robot consequently jumps the contact to the neighboring obstacle-piece of $\mathcal{B}_1$. The robot now follows the boundary of $\mathcal{B}_1$ until reaching a point where it detects a new obstacle $\mathcal{B}_2$ (Figure 2(b)). The double-contact configuration between $\mathcal{B}_1$ and $\mathcal{B}_2$ is a split vertex of $\mathcal{R}(\bar{\mathcal{B}})$. The robot can now proceed along two skeletal curves associated with two distinct θ-intervals, and continues along $\mathcal{B}_1$'s boundary as depicted in Figure 2(c). This motion eventually wedges the robot against two pieces of $\mathcal{B}_1$ and $\mathcal{B}_2$ (Figure 2(c)). The wedging configuration becomes a triple-contact vertex of $\mathcal{R}(\bar{\mathcal{B}})$. The vertex is incident to three skeletal curves associated with the three obstacles. The robot jumps the contact to $\mathcal{B}_2$, then proceeds to trace its boundary until reaching a second triple-contact

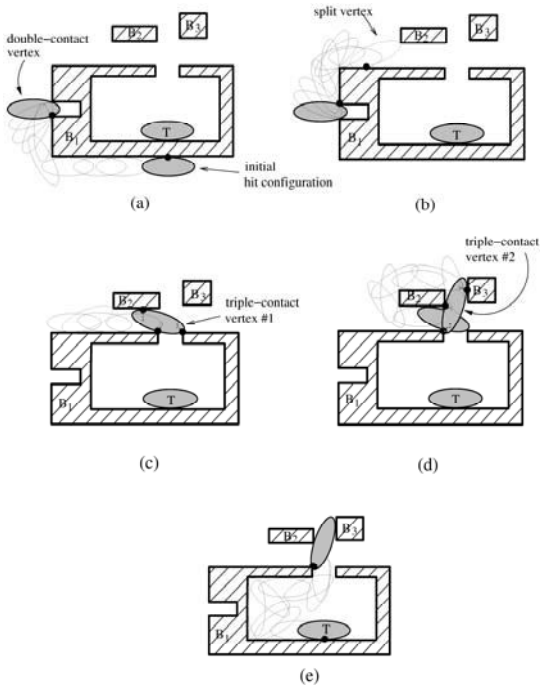

Fig. 2. (a) Arrival to an impassable gap. (b) Arrival to a split vertex. (c)-(d) Arrival to first and second triple-contact vertices. (e) Arrival to the target.

vertex of $\mathcal{R}(\bar{\mathcal{B}})$, this time associated with the three obstacles $\mathcal{B}_1$, $\mathcal{B}_2$, and $\mathcal{B}_3$ (Figure 2(d)). One of the skeletal curves emanating from the new vertex leads into the cavity formed by $\mathcal{B}_1$. The robot jumps the contact to $\mathcal{B}_1$, then proceeds to trace the internal cavity of this obstacle (Figure 2(e)). During this tracing the robot crosses the plane P containing S and T. However, the robot is further away from T at this configuration than at q_1. Hence it continues along the current skeletal curve. The current skeletal curve passes through two additional double-contact vertices associated with impassable gaps located at two concave corners of $\mathcal{B}_1$ (not depicted). The skeletal curve leads the robot along $\mathcal{B}_1$'s boundary until it reaches the plane P precisely at the target.

VI. CONCLUSION

The paper considered tactile-sensor based navigation of a three degrees-of-freedom mobile robot in an unknown planar environment. In particular, the paper focused on the robot's contact preserving paths where it attempts to efficiently circumnavigate a collection of impassable obstacles. These paths involve single or double-contact tracings. The paper provided a full characterization of the double-contact motions in terms of two types of c-space loops: contractible loops representing passable gaps, and non-contractible loops representing impassable gaps. Based on this classification, the paper identified a generic class of contact preserving paths consisting of single-contact tracings with efficient transitions at double-contact configurations involving impassable gaps, and at triple-contact configurations involving both passable and impassable gaps. A preliminary tactile-sensor navigation algorithm based on these paths was described and illustrated with an execution example.

The paper provides only a preliminary description of the tactile-sensor based navigation algorithm. A formal proof of correctness of the algorithm as well as realistic simulations and experimental validation will appear in a future paper. Two significant extensions of the current work are as follows. First, the c-space analysis of the robot's contact preserving paths relies on a decomposition of the polygonal obstacles into convex pieces. However, it is not clear wether this decomposition can be efficiently computed on-line by the robot. Second, as indicated in Section V, the tactile sensor can be replaced with a small-range sensor capable of reporting on obstacles lying within a disc enclosing the robot. Note that any simple small-range sensor, such as a rotating sonar beam, can provide these measurements. A challenging open problem is to establish techniques which would allow longer-range sensors, such as lasers and radars, to improve the algorithm's efficiency.

REFERENCES

[1] A. Arghir, J. Hertzberg, M. Devy, and F. Lerasle. Keep it simple, hybrid! a case study in autonomous office courier robot control. In *9'th Int. Symp. on Intelligent Robotic Systems (SIRS)*, pages 25–33, 2001.

[2] G. E. Bredon. *Geometry and Topology*. Springer-Verlag, N.Y., 1997.

[3] H. Choset and J. Burdick. Sensor-based motion planning: incremental construction of the hierarchical generalized voronoi graph. *The Int. J. of Robotics Research*, 19(2):126–148, 2000.

[4] H. Choset and J. Burdick. Sensor-based motion planning: the hierarchical generalized voronoi graph. *The Int. J. of Robotics Research*, 19(2):96–125, 2000.

[5] J. Cox and C.-K. Yap. On-line motion planning: Case of a planar rod. *Annals of Mathematics and Artificial Intelligence*, 3:1–20, 1991.

[6] J. M. Evans. Helpmate: an autonomous mobile robot courier for hospitals. In *IROS*, pages 1695–1700, 1994.

[7] Y. Gabriely and E. Rimon. C-space characterization of contact preserving paths with application to tactile-sensor based mobile robot navigation. Tech. report, Dept. of ME, Technion, http://robots.technion.ac.il/publications, June 2007.

[8] T. Hague, J. A. Marchant, and N. D. Tillet. Autonomous robot navigation for precision horticulture. In *Icra*, pages 1880–1885, 1997.

[9] J. Hopcroft and G. Wilfong. Motion of objects in contact. *Int. J. of Robotics Research*, 4(4):32–46, 1986.

[10] T. Huntsberger, Y. Cheng, A. Stroupe, and H. Aghazarian. Closed loop control for autonomous approach and placement of science instruments by planetary rovers. In *IEEE/RSJ Int. Conf. on Intelligent Robots and Systems (IROS)*, pages 3783–3790, 2005.

[11] I. Kamon, E. Rimon, and E. Rivlin. Tangentbug: A range-sensor based navigation algorithm. *Int. J. of Robotics Research*, 17(9):934–953, 1998.

[12] M. Keil and J. R. Sack. *Computational Geometry*. North-Holland, 1985.

[13] J.-C. Latombe. *Robot Motion Planning*. Kluwer Academic Publishers, Boston, 1990.

[14] S. L. Laubach, J. W. Burdick, and L. Matthies. An autonomous path planner implemented on the ROCKY7 prototype microrover. In *Icra*, pages 292–297, 1998.

[15] V. J. Lumelsky and A. Stepanov. Path planning strategies for point automaton moving amidst unknown obstacles of arbitrary shape. *Algorithmica*, 2:403–430, 1987.

[16] A. Phillips. Geometric theory of foliations (book review). *Americam Mathematics Monthly*, 96(1):71–76, 1980.

[17] A. Sankaranarayanan and M. Vidyasagar. Path planning for moving a point object amidst unknown obstacles in a plane: the universal lower bound on worst case path lengths and a classification of algorithms. In *Icra*, pages 1734–1941, 1991.

[18] B. Tovar, S. M. Lavalle, and R. Murrieta. Optimal navigation and object finding without geometric maps or localization. In *Icra*, pages 464–470, 2003.